ISSN (Print) 1226-1750
ISSN (Online) 2233-6656
Journal of Magnetics 24(4), 549-567 (2019) https://doi.org/10.4283/JMAG.2019.24.4.549

Magnetic Vortices and Skyrmions

Konstantin Y. Guslienko[1,2]*

[1] *Departamento de Física de Materiales, Universidad del País Vasco, UPV/EHU, 20018 San Sebastián, Spain*
[2] *IKERBASQUE, the Basque Foundation for Science, 48013 Bilbao, Spain*

(Received 8 December 2019, Received in final form 16 December 2019, Accepted 16 December 2019)

Recent advances in the research area of 2D magnetic topological solitons (vortices and skyrmions) in restricted geometries are reviewed. The description of the solitons is based on macroscopic micromagnetic approach and the Landau-Lifshitz equation of the magnetization motion. The vortex/skyrmion stability, energy barriers, gyrotropic and spin wave excitation modes in thin ferromagnetic films and dots are considered.

Keywords : magnetic vortex, magnetic skyrmion, topological charge, stability, spin waves

1. Introduction

Non-linear localized excitations are attracting the attention of physicists for a long time. Such excitations, including solitary waves or solitons, play an important role in quantum field theory, optics, condensed matter physics, etc. The solitons can be often classified by integer numbers (topological charges), which are preserved in their dynamics. The macroscopic equations of magnetization dynamics in ordered magnetic media are essentially nonlinear and allow a lot of soliton solutions including topological solitons. Topologically non-trivial magnetization configurations in ferromagnets, such as domain walls, bubble domains, vortices, and skyrmions are currently the focus of activity of researchers working in the area of solid-state magnetism.

In this review I consider 2D magnetic topological solitons – vortices and skyrmions. Such magnetic solitons possess intriguing and novel properties due to their topologically non-trivial magnetization configurations. I account for the papers on magnetic vortices published in 2007-2019 and recent papers on magnetic skyrmions in restricted geometry. Review of the papers in the area of magnetic vortices published by the end of 2006 was conducted in Ref. [1].

The paper is organized as follows. The definition of the topological charges of the magnetic vortices and skyrmions is presented in Sec. 2. Static and slow dynamics behavior of magnetic vortices are considered in Sec. 3. The fast linear and nonlinear vortex dynamics are considered in Sec. 4. The classification of the magnetic skyrmions is done in Sec. 5. Stabilization of the individual skyrmions by the Dzyaloshinskii-Moriya exchange interaction (DMI) and magnetostatic interaction is considered in Sec. 6. The emergent electromagnetic field generated by the skyrmion magnetization texture, its consequences, low and high frequency spin excitation modes on the skyrmion background are considered in Sec. 7. The review is concluded by a Summary in Sec. 8.

2. 2D Magnetic Topological Solitons: Vortices and Skyrmions

The magnetic vortices and skyrmions are kind of magnetic topological solitons [2] in 2D spin systems characterized by an integer skyrmion number (topological charge) defined by

$$N = \frac{1}{4\pi}\int d^2\mathbf{r}\ \mathbf{m}\cdot\left(\frac{\partial \mathbf{m}}{\partial x}\times\frac{\partial \mathbf{m}}{\partial y}\right), \quad (1)$$

where the soliton magnetization represented by the unit vector $\mathbf{m}$ ($\mathbf{m}(\mathbf{r}, t) = \mathbf{M}(\mathbf{r}, t)/M_s$), M_s is the saturation magnetization) and $\mathbf{r} = (x, y)$ are in-plane spatial coordinates. It represents the number of times that the vector $\mathbf{m}$ wraps the unit magnetization sphere $\mathbf{m}^2 = 1$ changing the spatial coordinates.

We parameterize the unit magnetization vector by the spherical angles, $\mathbf{m} = \mathbf{m}(\Theta, \Phi)$. The angles Θ, Φ are functions of the polar radius vector $\boldsymbol{\rho} = (\rho, \varphi)$ located in the

*Corresponding author: Tel: +34-943-018205
e-mail: kostyantyn.gusliyenko@ehu.eus

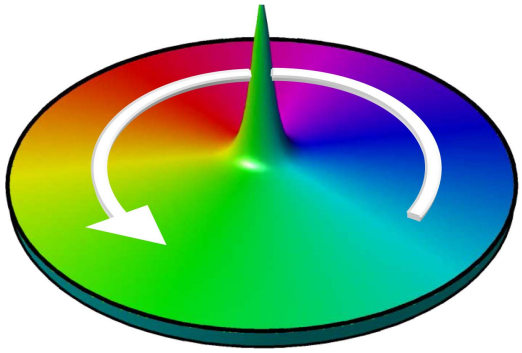

Fig. 1. (Color online) Magnetic vortex in a thin cylindrical dot. The magnetization rotates counterclockwise in the dot plane. The core magnetization direction is upward (vortex polarity $p = +1$). (courtesy by S.-K. Kim)

film or dot plane, and z-axis is normal to the plane. We consider cylindrically symmetric magnetization configurations (**m** depends only on the radial coordinate ρ), with the z-component defined by the angle $\Theta(\rho)$. The skyrmion number (1) for the radially symmetric solitons having the in-plane magnetization angle $\Phi = q\varphi + \Phi_0$ is $N = q(p - \cos\Theta(R))/2$, where $\cos\Theta(\rho = 0) = p = \pm 1$ is the soliton core polarity, $q = \pm 1$ is a magnetization vorticity. The vorticity is $q = +1$ for magnetic vortex/skyrmion or $q = -1$ for antivortex/antiskyrmion. For magnetic vortices/antivortices $\cos\Theta(\rho = R) = 0$ and the charge is $N = qp/2$ half-integer, whereas for skyrmions/antiskyrmions $\cos\Theta(\rho = R) \approx -p$ and the charge $N = qp$ is integer and equal to ± 1. We consider below only the vortices and skyrmions with the vorticity $q = 1$. The parameter R stands for the system in-plane size. In finite magnetic systems such as dots, stripes etc., the skyrmion number can be non-integer due to restricted area of the integration in Eq. (1) and essential contribution of the magnetostatic energy and/or DMI. The angle Φ_0 is the soliton chirality or helicity. It is equal $\pm \pi/2$ for magnetic vortices and Bloch skyrmions and 0, π for Neel skyrmions.

Magnetic vortices (Fig. 1) with the core size about 10 nm are non-localized topological solitons [2], because the magnetization field is inhomogeneous at infinite distance from the vortex center. Whereas the magnetic skyrmions with radii down to several nm are localized topological solitons [2], their magnetization becomes uniform at infinity. Both magnetic vortices and skyrmions are magnetization textures on the nanoscale, which behave as particles that can be moved, created and annihilated.

3. Static Properties of Magnetic Vortices

3.1. Single layer dots

Magnetic vortices in soft magnetic nanodots have been extensively studied during several decades both for their applied (non-volatile information storage and spin-transfer torque oscillators) as well as fundamental value. The vortices are the dot ground state for a wide range of the circular dot thickness L and radii R [1]. The magnetic energy has a deep minimum in the vortex state for values of R of several hundred nm and zero magnetic field, *i.e.*, the vortices are extremely stable for values of R of several hundred nm. When the dot radius R is close to the exchange length of magnetic material (around 20 nm), its magnetic configuration becomes markedly different from the vortex state. There are regions of stability/metastability of C-type and "leaf" magnetization states [3]. It was shown recently [4] that there is another vortex ground state with large radius-dependent core in nano-scale dots of several exchange lengths in size. Its energy was computed numerically and its stability was studied analytically that allowed to plot a detailed magnetic phase diagram [4]. Large vortices may co-exist with the classical ones, while being separated by an energy barrier, controllable by tuning the dot geometry and material.

3.2. Vortex ground state and reversal in layered F/N/F and F/N/AF dots

An analytical model of magnetization reversal via vortex nucleation and annihilation in double-layer ferromagnetic/antiferromagnetic cylindrical dots was developed in Refs. [5, 6]. The coupling of the ferromagnet to antiferromagnet was modeled by means of an interfacial unidirectional exchange field. The nonuniformity of the magnetization reversal mode along the dot thickness was explicitly accounted and resulted in a tilted vortex core (tilted Bloch line). The vortex annihilation fields, the vortex trajectory, and the average dot magnetization are calculated as functions of the dot geometrical parameters and the external field direction with respect to the exchange-bias field. The vortex core tilt resulted in an asymmetry of the nucleation and annihilation fields. This asymmetry was calculated explicitly as a function of dot thickness and radius.

The equilibrium magnetization configurations of trilayer circular nanopillar were calculated within micromagnetic approach [7]. Nanopillar was assumed to be a vertical stack of ferromagnetic/nonmagnetic/ferromagnetic layers. The regions of geometrical parameters of nanopillar (radius and thickness), where the magnetic vortices and single domain states appear in the ground state, were calculated analytically and checked by simulations. A considerable influence of thicknesses of the ferromagnetic layers and spacer on the stability of vortex states was found. The calculations demonstrated the essential role of

the interlayer magnetostatic coupling in formation of the vortex and single–domain states in the layered nanopillars. The results can be applied to interpret experiments on spin torque induced magnetization dynamics in nanopillars and tunnel junctions.

3.3. Vortex energy barriers

There is strong dependence of the stable, metastable energy minima and energy barriers on the magnetic field and dot geometrical parameters. The effect of the in-plane magnetic field and temperature on the vortex nucleation in 2D permalloy (NiFe alloy) dot arrays was investigated both experimentally and theoretically [8, 9]. Time decay of the magnetization of the arrays of permalloy circular dots was measured on a long-time scale (hours) near the vortex nucleation field [8]. A considerable influence of external magnetic field and temperature on the slow magnetization dynamics was detected. The observed effects were explained by overcoming the field dependent energy barriers in the process of vortex nucleation. The magnetization time decay of the dot array was calculated and information about the energy barriers and their field dependence was extracted.

Time evolution of the ferromagnetic resonance output signal in the arrays of thin permalloy circular dots of submicron sizes was measured near the critical fields of the vortex nucleation and annihilation [9]. Surprisingly short times of the transition from quasi-uniform to the vortex magnetization state (several milliseconds) were detected. The observed effects were explained by overcoming the field dependent energy barriers in the process of vortex core nucleation/annihilation. The energy barrier values found from time dependences of the resonance peak intensities were compared with ones calculated within the rigid vortex model (RVM). The RVM overestimates the nucleation barriers related to the vortex core penetration to the dots. The switching time from the vortex to saturated state is also quite short, but can be successfully described within RVM.

The research demonstrated an essential role of the field dependent energy barriers in the long-time vortex nucleation dynamics. The obtained results can serve as a basis for understanding of the magnetization reversal and the thermal stability in the vortex state dot arrays.

4. Vortex Dynamics

4.1. High order gyrotropic modes and vortex mass

New modes of the vortex magnetization oscillations in thick ferromagnetic nanodots were predicted theoretically on the base of the Landau-Lifshitz equation of the magnetization motion and observed by broadband ferromagnetic resonance [10, 11]. The modes are related to the thickness dependent vortex gyrotropic dynamics. These exchange-dominated modes are flexure oscillations of the vortex core string with $n = 0$, 1, 2 nodes of the dynamical magnetization along the dot thickness (50-100 nm). The 1st order ($n = 1$) gyrotropic mode was detected in permalloy nanodots for the first time using broadband ferromagnetic resonance technique in the GHz frequency range [10]. The frequency of the $n = 0$ mode was explained introducing the vortex mass, which has considerable value for thick dots [12]. The vortex mass is a result of interaction of the moving vortex core with azimuthal spin waves having azimuthal indices $m = \pm 1$. The intensity of the mode with $n = 1$ in some cases is higher than the one of the quasi-uniform mode with $n = 0$. This opens promising perspectives in the area of spin transfer torque oscillators allowing to increase essentially their microwave generation power [13]. Accounting that the uniform gyrotropic mode is already used as a excitation mode of the vortex spin torque oscillators in layered nanopillars and nanocontacts with a thin ferromagnetic layer, the observed spin vortex modes can be implemented in the next generation of spin-torque nanoscale devices.

4.2. Vortex gyrotropic modes in coupled dot arrays (linear dynamics)

Broadband ferromagnetic resonance in square arrays of permalloy circular dots with different interdot separations was measured in the vortex ground state [14]. The interdot separation was kept sufficiently large to avoid a transition of the dots in the single domain state [15]. The detected spin excitations showed a complicated dependence of their frequencies on the interdot coupling strength. A considerable influence of the interdot separation on the gyrotropic vortex frequency and splitting of the azimuthal spin wave frequencies with indices $m = +1/-1$ was detected. The gyrotropic frequency and the first azimuthal doublet frequency splitting depend non-monotonously on the interdot spacing, whereas the dependence of the second doublet frequency splitting on this parameter is monotonous. The observed effects were explained by the influence of the dipolar and quadrupolar contributions to the dynamic interdot magnetostatic interactions.

The low frequency dynamics of two coupled magnetic vortices oscillating in a pair of laterally patterned circular dots were calculated [16, 17]. The linearized Thiele equations of motion of the vortex core positions [1] were applied to describe the dynamics. The main emphasis was put on the symmetry of the excited spin eigenmodes and the possibility to excite them by applying the variable

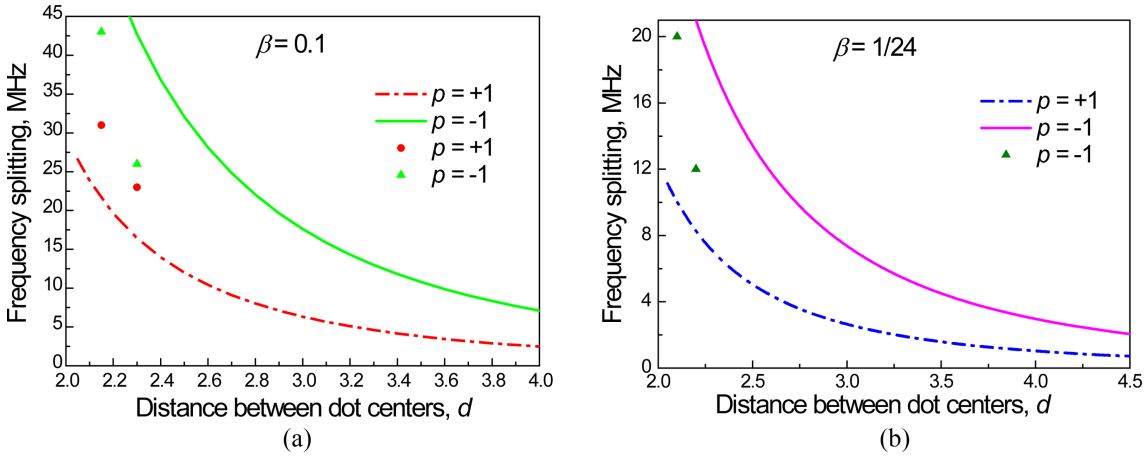

Fig. 2. (Color online) Calculated (solid and dashed lines) dependences of the frequency splitting of the vortex gyrotropic modes in dot pair on the interdot distance $d = D/R$. The dot aspect ratio, height/radius $\beta = h/R$: a) $\beta = 0.1$; b) $\beta = 1/24$ [17]. The triangles and circles correspond to the positive/negative product of the dot polarities $p = p_1p_2 = +1/-1$, respectively, and are taken from the experiments (a) by Sugimoto *et al.* [18] and (b) by Jung *et al.* [19].

driving magnetic fields in different directions. The importance of the high-order multipole terms in the interdot coupling energy decomposition was underlined and recent experiments on the coupled magnetic vortex dynamics in patterned films were interpreted. Using the expression for frequency splitting of the eigenmodes [17], one can plotted it for different dot aspect ratios taken from the experiments [18, 19] in Fig. 2. The frequency splitting is higher for the pair of magnetic dots with different vortex core polarities ($p_1p_2 = -1$). There is quite good agreement between the theoretical and experimental results in Fig. 2 (a, b). The pole free model describes well the frequencies of isolated dot, but for dot pair it gives the results a little different from experimental ones. This is because some surface charges are generated that are not accounted in the model.

If the eigenmodes [17] of a magnetic vortex dot pair are excited in one dot, then due to interdot coupling the vortex core motion is excited in the second dot. Such interacting vortices behave as the system of coupled oscillators showing the typical for such systems energy transfer as was reported by Jung *et al.* in Ref. [19]. The time τ of the transfer of the total energy from one magnetic dot to another is inversely proportional to the frequency splitting, $\tau = \pi/\Delta\omega$ ($\Delta\omega = \left|\omega_1^p - \omega_2^p\right|$). τ is a time delay between two maxima of vortex oscillations in two dots $\mathbf{X}_1(t)$ and $\mathbf{X}_2(t)$. This time is order of 10 ns and can be reduced increasing the dot aspect ratio $\beta = h/R$.

For application of the vortex state dots for transferring the microwave signal (*e.g.*, in magnonics) the efficiency of energy transfer from first dot to the second is important. The amplitude of gyration in the second dot $\left|\mathbf{X}_2\right|_{t=\tau}$ induced by vortex gyration in the first dot $\left|\mathbf{X}_1\right|_{t=0}$ can be described by taking into account the oscillations damping $\left|\mathbf{X}_2(\tau)\right| \propto \left|\mathbf{X}_1(0)\right| \exp(-\Gamma\tau)$, where $\Gamma = d_0\omega_0$, $d_0 = \alpha(5/8 + \ln(R/R_c)/2)$, α is the damping parameter, R_c is the vortex core radius, and eigenfrequency is $\omega_0 = (20/9)\gamma M_s\beta$. The efficiency of the transfer $\exp(-\Gamma\tau)$ is determined mainly by the damping parameter and the dot aspect ratio β. The amplitude of gyration in the second dot induced by initial amplitude in the first dot due to interdot magnetostatic coupling is shown in Fig. 3. Decreasing the parameter α (e.g., choosing NiMnSb with $\alpha = 0.0023$ instead of Py with $\alpha \approx 0.008$) one can obtain better transfer between dots. The time for transferring the total magnetic energy from one dot to another is inversely proportional to the

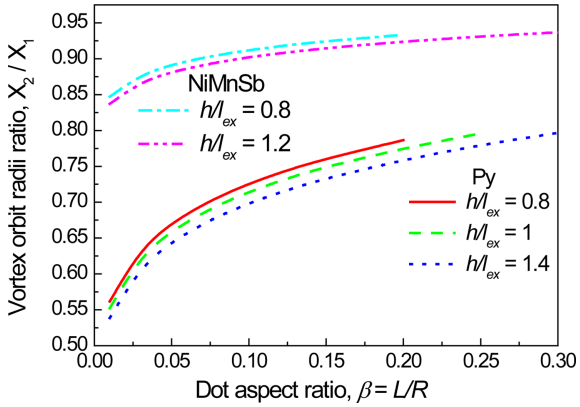

Fig. 3. (Color online) The amplitude of gyration in the second dot X_2 in a dot pair relatively to initial amplitude in the first excited dot X_1 depending on the dot aspect ratio for different dot thicknesses h/l_{ex} (l_{ex} is the exchange length). Distance between the dot centers is $d = D/R = 2.1$.

dot aspect ratio. Therefore, the faster energy transfer can be achieved by increasing thickness to radius ratio.

The low-frequency excitations of magnetostatically coupled vortices can be calculated in a dot array, for instance in a square vortex $N \times N$ lattice with N about of 1000. Special cases of the clusters of 3, or 4 interacting dots were also considered [20]. The general multipole expansion of the magnetostatic interaction energy between non-uniformly magnetized particles was developed [17]. Then, the calculations were applied to a particular case of lateral arrays of the interacting vortex state dots [one- and two-dimensional (2D) square and hexagonal lattices]. The odd rank multipole moments (dipolar, octupolar, etc.) play the main role in the interdot magnetostatic interaction. The vortex collective frequencies and group velocities were calculated within the pole-free and rigid vortex models and compared with the experimental observations of the dynamics by broadband ferromagnetic resonance and X-ray imaging. The cases of different vortex core polarities were considered, and their strong influence on the excitation spectra was shown. Frequency bandwidths of the vortex gyrotropic modes for dense 2D square (Fig. 4) and hexagonal arrays can exceed 1/3 of the eigenfrequency of an isolated dot. The group velocity for transferring the total microwave magnetic energy from one dot to another was found to be proportional to the dot thickness and inversely proportional to the squared dot lattice period. This group velocity is anisotropic as function of the wave vector **k** direction in the patterned film plane and decreases with the modulus |**k**| increasing (see Fig. 4b). The obtained results can serve as a basis for understanding of the propagation of spin excitations in 2D magnonic crystals consisting of the vortex state magnetic dot arrays.

4.3. Vortex and anti-vortex domain walls in magnetic stripes

The magnetic field (or electric current) driven domain-wall (DW) motion in magnetic nanostripes is of considerable interest because it is essential to the performance of information-storage and logic devices. One of the key problems is to understand the complex behaviors of oscillatory domain-wall motions under applied magnetic fields stronger than a critical field (Walker field), above which the velocity of domain walls markedly drops. In a certain range just above the Walker field, the motions are not chaotic but rather periodic with different periods of dynamic transformations of a moving domain wall between the different types of its internal structure [21]. Three simulated types of the periodic dynamic transformations consist of different types of domain-wall patterns that are transformed from one type to another. The transformation periods vary with the field strength and the nanostripe sizes.

The motions of domain walls in soft magnetic nanostripes were calculated analytically [22]. The DWs exhibit steady and transient motions in the low fields and oscillations of their internal structure above a critical field. The developed analytical model of the domain walls explained their dynamics by the motions of a limited number of magnetic topological solitons having nonzero gyrovectors such as vortex and antivortex. The model predicts the reduced DW velocity and critical field in the low-field regime, and increased wall-oscillation frequency in nanostripes, compared to the Walker solution for bulk magnets. The critical field and velocity are determined by the nanostripe thickness and width, whereas the oscillation frequency depends only on the field strength.

The dynamic transformations of the internal structure of

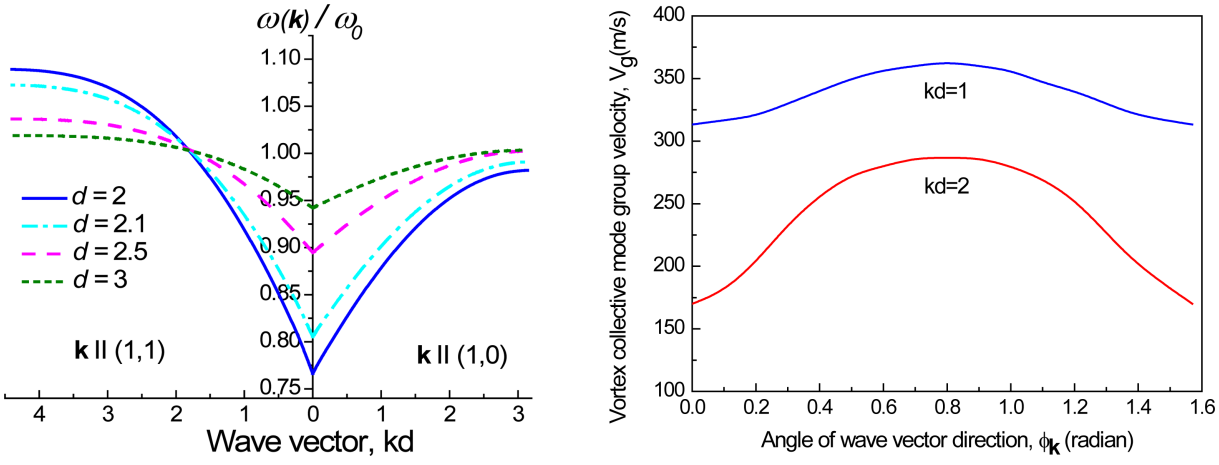

Fig. 4. (Color online) Gyrotropic frequency dispersion [17] and group velocity ($d = 2.1$) of the vortex collective modes in square array of the permalloy cylindrical dots. ω_0 is gyrofrequency of the isolated dot. The interdot distance $d = D/R$, D is the lattice period, R is the dot radius. The angle $\phi_{\mathbf{k}}$ of the wave vector **k** is counted from [10] direction in the square dot lattice.

a moving domain wall in magnetic nanostripes, driven by applied magnetic fields larger than the Walker field strength, H_w, were simulated in detail in Ref. [23]. It was found that one of the edge-soliton cores of a transverse wall should reach a critical nucleation size by moving inward beyond a critical deviation, Y_c, in the transverse direction, in order to secure the transformation from a transverse to a vortex or antivortex wall. The value of Y_c is estimated to be close to the vortex/antivortex core radius. Upon completion of the nucleation of the vortex (antivortex) core, the vortex (antivortex) domain wall is stabilized, accompanying its characteristic gyrotropic motion in a potential well (hill) within the nanostripe.

4.4. Vortex core reversal and non-linear vortex dynamics

Understanding the physical origin of vortex core reversal is the key to the effective manipulation of the dynamic switching of core orientation via the choice of appropriate strengths and frequencies of driving forces as well as of magnetic nanoelement geometry. The magnetic vortex can be used, through its downward or upward core orientation, as a memory unit for information storage, and thus, controllable core switching deserves a special attention.

The vortex core reversal was experimentally detected in permalloy dots by X-ray imaging in Ref. [24]. Micromagnetic numerical studies on the strong radiation of spin waves produced by the reversal of a magnetic vortex core (VC), as well as their injection and propagation in magnetic nanowires were conducted in Ref. [25]. It was found that the radial spin waves can be emitted intensively from a reversed VC and then can be injected into a long nanowire (Fig. 5). These results offered a preview of the generation, delivery, and manipulation of intensive spin waves in magnetic elements, which are applicable to information-signal processing in potential spin wave devices.

Electric current driven VC reversal and the accompanying spin-wave emission, driven by spin-polarized ac currents in permalloy nanodots were simulated in Ref.

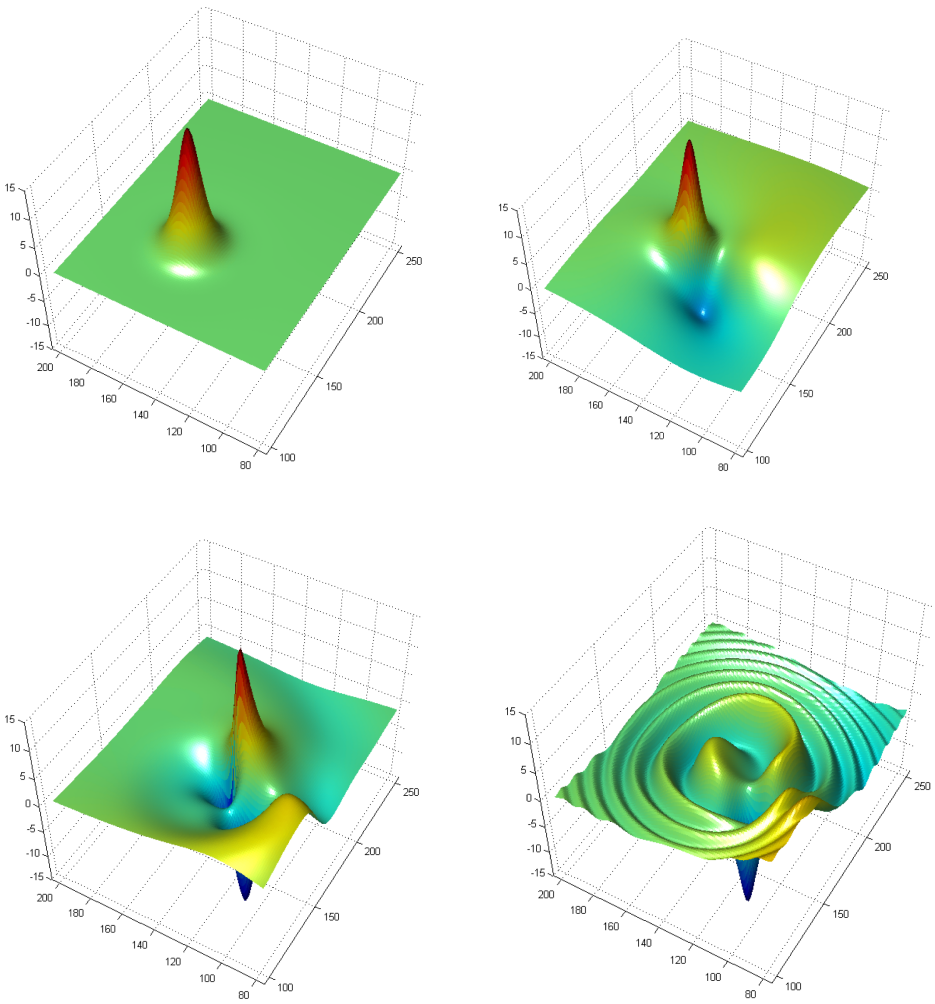

Fig. 5. (Color online) The time evolution of the vortex magnetization in course of the vortex core reversal [25, 27]. The reversal is accompanied by emission of the radial spin waves [25]. (courtesy by S.-K. Kim)

[26]. It was found that the VC polarization is effectively switchable between its upward and downward bi-states and controllable by applying current above its threshold density, but with sufficiently small magnitude at frequencies close to the vortex eigenfrequency. This VC reversal occurs through the creation of a vortex-antivortex pair and the subsequent annihilation of the initial vortex and the created antivortex, when the velocity of the initial VC reaches its critical value of approximately 300 m/s. The strong spin waves are emitted immediately after the VC switching. These pioneering results provided the means to manipulate bi-state VC orientations by spin-polarized currents.

To clarify the mechanism of ultrafast VC reversal, simulations of the magnetic vortex dynamics were conducted in permalloy cylindrical dots under an oscillating in-plane magnetic field over a wide range of the field frequency and amplitude [27]. The simulations revealed different kinds of the nontrivial dynamic responses of vortices to the driving external field, including the VC reversal. In particular, the results offer insight into the 10 ps scale underlying physics of the ultrafast VC reversal driven by small-amplitude (about of 10 Oe) oscillating fields. Analytical and micromagnetic calculations conducted in Ref. [28] revealed that the origin of vortex core reversal is a dynamical gyrotropic field. This field is induced by vortex motion, concentrated near the deformed vortex core and is proportional to the velocity of the moving vortex. The VC switching occurs whenever the velocity of vortex core motion reaches its critical velocity. These pioneering works provided fundamentals of how to effectively manipulate the dynamical switching of the VC orientation.

A spin-wave theory explaining experimentally observed frequency splitting of the spin waves with azimuthal symmetry of a magnetic dot in a vortex ground state was developed in Ref. [29]. A theoretical approach in which all dynamic eigenmodes of the vortex-state magnetic dot are described within a unified perturbative scheme was suggested. The splitting is a result of the dipolar hybridization of three spin-wave modes having azimuthal indices $m = +1/-1$: two high-frequency azimuthal dipolar modes with indices $m = +1/-1$ and a low-frequency gyrotropic mode, describing translational motion of the vortex core and having index $m = +1$. The calculated magnitude of the frequency splitting is proportional to the ratio of the dot thickness to its radius. The calculated frequency splitting is in good quantitative agreement with the results of time-resolved Kerr pump-probe measurements performed by different experimental groups.

The concept of universal criterion for ultrafast vortex-

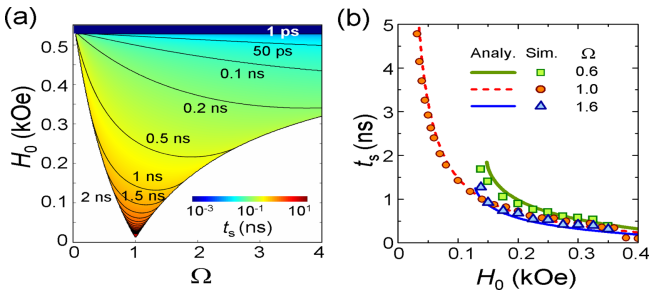

Fig. 6. (Color online) (a) Contour plot of the simulated vortex core switching time in Ω – H_0 plane [30]: (b) Calculated and simulated vortex core switching time as function of the magnitude of oscillating in-plane field $H_0(\omega)$. The gyrotropic frequency $\omega_G/2\pi$ =580 MHz, $\Omega = \omega/\omega_G$. Permalloy dot with R = 150 nm and L = 20 nm.

core switching between the up- and down-core bi-states in soft magnetic nanodots was numerically confirmed in Ref. [30]. It was established that the VC critical velocity is $v_c = 1.66\gamma\sqrt{A}$ (about of 330 m/s for permalloy), with the exchange stiffness A and the gyromagnetic ratio γ. Based on this criterion, phase diagrams of the VC switching and the switching time with respect to the frequency and amplitude of the circularly rotating magnetic field were derived (Fig. 6).

Microwave spectroscopy of individual vortex-state magnetic nanodots in out-of-plane bias magnetic field H was performed using magnetic resonance force microscopy [31]. It revealed the splitting induced by H of the gyrotropic frequency of the vortex core gyration related to the existence of the two stable core polarities. This splitting enables spectroscopic detection of the core polarity. The bi-stability extends up to a large negative (antiparallel to the core magnetization) value of the bias magnetic field, at which the core polarity is reversed. The difference between the frequencies of the two stable vortex gyration modes corresponding to each core polarity is proportional to H and to the ratio of the dot thickness to its radius. Simple analytic theory in combination with micromagnetic simulations supplied a quantitative description of the observed bi-stable vortex dynamics.

A time-resolved X-ray imaging (time-resolved photoemission electron microscopy) and micromagnetic simulations of the magnetic vortex dynamics in the nonlinear regime in patterned permalloy dots were reported in Ref. [32]. It was shown that the vortex core shifts beyond 20 %-25 % of the dot radius, the initial motion is characterized by essential distortions of the vortex magnetization configuration, a transient cross-tie domain wall state, and instabilities in the vortex core polarity that influence the vortex core trajectories.

For a circular magnetic nanodot in a vortex ground

state, the critical velocity v_c of the VC reversal dependence on the magnitude H of out-of-plane magnetic field was studied in Ref. [33]. It was found that, similarly to the case $H = 0$, the critical velocity does not depend on the size of the dot. The critical velocity is dramatically reduced when the bias field opposite to the VC direction approaches the value, at which a static core reversal takes place. A simple analytical model showed a good agreement with numerical results. The numerical study has demonstrated that there are two contributions to the process of the VC reversal as follows: the static reversal mechanism related to the instability of VC with polarity directed against the bias field and the dynamical reversal mechanism related to VC deformation. While the first mechanism keeps the axial symmetry of the vortex magnetization, the second one breaks this axial symmetry and creates an "easy" VC reversal path. Thus, the bias magnetic field applied oppositely to the vortex core direction facilitates the dynamical reversal process [33].

The quasi-stationary and transient (nanoseconds) regimes of nonlinear vortex dynamics in a soft magnetic dot driven by an oscillating external field were studied in Ref. [34]. A nonlinear dynamical system of equations for the VC position and phase was derived assuming that the main source of nonlinearity is the magnetostatic energy. In the stationary regime, the occurrence of a fold-over bifurcation was demonstrated and the resonant nonlinear vortex frequencies were calculated analytically. In the transient regime the VC dynamics can be described by an oscillating trajectory radius. The resulting dynamics contain multiple frequencies with amplitude decaying in time. The ranges of the system parameters leading to VC instability (core polarity reversal) were evaluated [34].

The anharmonicity of the potential well confining magnetic VC in a nanodot was measured by magnetic resonance force microscope (MRFM) in Ref. [35]. The stray field of the MRFM tip was used to displace the equilibrium VC position away from the nanodot center. The anharmonicity is then inferred from the relative frequency shift of the eigenfrequency of the VC translational mode. An analytical framework was proposed to extract the nonlinear coefficient. Traces of these frequency shifts were recorded while scanning the tip above an isolated FeV nanodot. An 10 % increase of the VC frequency was observed when the equilibrium position of the VC is displaced to about one-third of its radius. This calibrates the tunability of the vortex gyrotropic mode by external magnetic field [35].

Detailed micromagnetic simulations of magnetization dynamics of a vortex state in the free layer of a circular nanopillar excited by the spin transfer torque of the spin-polarized current were reported in Ref. [36]. The magnetization of the reference layer (polarizer) was assumed to be fixed. Changing the applied current density, different behaviors of magnetization were found for the thin layer which was initially in the vortex state. A new regime of the dynamic magnetization response to the current was reported: VC expelling from the dot, subsequent in-plane magnetization oscillations in single domain state, and the vortex return with an opposite core polarity. Absence of a vortex-antivortex pair formation was justified by the VC arriving to the dot border before it reaches the critical velocity of the VC reversal. The gyrotropic frequency is too small to reach the critical velocity for the VC reversal inside the particle. The ultimate VC velocity was below 330 m/s, the calculated in Refs. [28, 30] critical velocity for a vortex-antivortex pair formation. The orbit radius of the vortex steady gyrotropic motion strongly depends on the current value. Conditions of the vortex state as a nano-oscillator to achieve steady magnetization oscillations corresponding to VC gyrotropic motion were analyzed. These conditions are formulated via the critical currents and vary essentially with the damping parameter and the cell size used for simulations.

The main parameters of the spin polarized current induced magnetic vortex oscillations in nanopillars were calculated in Ref. [37], such as the range of current density, where vortex steady oscillations exist, the oscillation frequency and orbit radius. The non-linear vortex frequency and non-linear vortex damping were taken into account. To describe the vortex excitations by the spin polarized current a generalized Thiele approach to motion of the vortex core was used accounting the Slonczewski spin torque. The spin polarized current induced magnetic vortex dynamics in tri-layer nanopillars of ferromagnet/non-magnetic spacer/ferromagnet with two oscillating ferromagnetic layers were calculated in Ref. [38]. In particular, the critical currents of the vortex steady oscillations and the oscillation frequencies were found. All the calculation results [37, 38] were represented via the nanopillar layer sizes, saturation magnetization, and the Gilbert damping.

It was shown that a steady VC gyrotropic motion in a vortex-state free layer of a magnetic nanopillar driven by a spin-polarized current can be quantitatively described in the framework of the standard model of non-isochronous auto-oscillator [39]. The parameters of the vortex auto-oscillator, determining its non-autonomous dynamics and synchronization properties, can be found from the experimentally measured linewidths of higher harmonics of the generated microwave signal. The presented results demonstrated that vortex spin-torque nano-oscillators, having low generation linewidth and relatively high output power,

can be strongly non-isochronous, and, therefore, could be prospective candidates for mutual synchronization in large oscillator arrays.

The detailed theoretical description of the vortex spin-torque oscillators was developed [13], where nonlinear vortex dynamics in a circular magnetic nanodot induced by a spin-polarized current was investigated analytically and numerically. A generalized nonlinear Thiele equation including spin-torque term was used for describing the VC core transient and steady orbit motions and nonlinear contributions to all forces in this equation were analyzed. Blue shift of the nano-oscillator frequency increasing the current was explained by a combination of the exchange, magnetostatic, and Zeeman energy contributions to the frequency nonlinear coefficient. Applicability and limitations of the standard nonlinear nano-oscillator model [40, 41] were established. The complicated spin dynamics in a circular vortex state dot in response to the spin polarized current was simulated in Ref. [42].

4.5. Spin-waves in the vortex ground state

Linear spin dynamics in the vortex state of permalloy cylindrical dots subjected to an in-plane bias magnetic field was reported in Ref. [43]. It was demonstrated by a broadband ferromagnetic resonance technique and by simulations that breaking the cylindrical symmetry of the magnetic vortex gradually changes and suppresses the azimuthal spin eigenmodes below the vortex nucleation field and leads further to the appearance of new spin eigenmodes. The parallel microwave field pumping was shown to be a unique tool to observe spin excitation modes localized near the strongly displaced VC core for the bias field between the vortex nucleation (H_n) and annihilation (H_{an}) fields (Fig. 7). Meanwhile, the perpendicular field pumping, which excites the spin waves

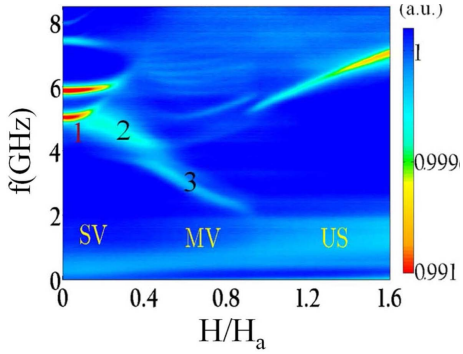

Fig. 7. (Color online) The vortex excitation modes measured by broadband ferromagnetic resonance (parallel microwave field pumping) vs. in-plane magnetic field [43]. Permalloy dots with $L = 25$ nm and $R = 518$ nm. Numbers 1, 2, 3 label the modes discussed in the text.

throughout the entire dot, reveals a crossover between two dynamic vortex regimes near the nucleation field.

The spin-wave eigenmodes (n, m) classification based on the number of nodes in radial and azimuthal directions could be applicable only below the vortex nucleation field (see Fig. 7). The spin-wave mode frequencies vary in qualitatively different way as the vortex is shifted from the dot center to the dot edge for the parallel and perpendicular excitation schemes. An experimental proof that the main azimuthal modes (with the indices $m = +1/-1$, $n = 0$, no radial nodes, the modes #1) exist only in low fields, below H_n, was supplied. A spin wave mode of the shifted vortex excited by using parallel pumping was observed (mode #2). This mode splits out from the lowest azimuthal mode (with $m = +1$) and is a superposition of the azimuthal modes with the indices $m = +2/-2$ rotating around the vortex core in the opposite directions. Furthermore, a high-field soft mode localized near the vortex core for parallel pumping was observed (mode #3). This mode can be approximately described as having a wave vector along the bias field and is stable up to H_{an}. The fundamental differences in the field dependence of spin-wave modes excited with *perpendicular* (abrupt change between the stable and metastable vortex regions, broad spin-wave response in the metastable vortex state) and *parallel* (the spin-wave spectrum transforms more continuously, a single localized mode in the vortex metastable state) pumping were found [43].

Detailed broadband ferromagnetic resonance measurements of the azimuthal and radial spin waves in circular permalloy dots in the vortex ground state were reported [44]. The dots with aspect ratio height over radius β varied from 0.03 to 0.1 were explored. The frequency splitting of two lowest azimuthal modes ($n = 0$, 1, $m = +1/-1$) was observed. The observed dependence of the frequency splitting on β was reasonably well described by the dynamic splitting model [29] accounting the azimuthal spin waves and vortex gyrotropic mode interaction.

A topological gauge vector potential which influences spin-wave excitations over a nonuniform, slowly moving magnetization background was introduced in Ref. [45]. The gauge vector potential was represented by time and spatial derivatives of the nonuniform magnetization. The time component of the potential plays a principal role in the magnetization dynamics of typical nanostructures. As an example, spin modes excited in the vortex-state magnetic dots were considered. The vortex/spin-wave interaction was described as a consequence of the gauge field arising due to the moving vortex magnetization. The approach yields a giant frequency splitting of the spin waves having nonzero overlapping with the vortex background

mode as well as a finite vortex mass of dynamical origin. Increasing amplitude of the azimuthal spin waves leads to an instability of the vortex background.

The magnetization dynamics in circular permalloy dots with spatially separated magnetic vortices interconnected by Neel domain walls (double vortex state) was investigated in Ref. [46]. A novel type of quasi one-dimensional (1D) localized spin wave modes confined along the domain walls, connecting each of two vortex cores with two edge half-antivortices, were identified. Variation of the mode eigenfrequencies with the dot sizes is in quantitative agreement with the developed model, which considers a dipolar origin of the localized 1D spin waves.

The excitation of spin-wave eigenmodes in the vortex state of ferromagnetic circular dots made of permalloy was examined both theoretically and experimentally using Brillouin light scattering microscopy [47]. The radial spin-wave eigenmodes of single elements with high mode numbers (up to $n = 13$ for the largest dot radius 2.5 μm) were detected. An equation for the eigenfrequencies valid for arbitrary dot thickness/radius ratio was obtained within the magnetostatic approximation. The influence of the dot radius on the spatial mode profiles, in particular, changes in the pinning of the dynamical magnetization at the edges and in the center of the dots, was demonstrated. The measured spin-wave eigenfrequencies are in good agreement with the analytical calculations for the dots with different radii.

Broadband magnetization response of coupled vortex state magnetic dots in layered nanopillars was explored as a function of in-plane magnetic field and interlayer separation [48, 49]. For the dipolarly coupled circular Py/Cu/Py nanopillars, a small in-plane field splits the eigenfrequencies of azimuthal spin wave modes inducing an abrupt transition between in-phase and out-of-phase kinds of the low-lying coupled spin wave modes. The critical field for this splitting is determined by antiparallel chiralities of the vortices in the layers.

There are two stable competing magnetization configurations of the circular dot in the in-plane magnetic field smaller than the vortex annihilation field: the vortex and the quasi-uniform (C-state). The microwave absorption properties in an array of non-interacting permalloy dots in the frequency range 1-8 GHz were measured in Ref. [50] varying the in-plane bias magnetic field in the region of the dot magnetization state bi-stability. It was found that the microwave absorption properties in the vortex and quasi-uniform stable states are substantially different, so that switching between these states in a fixed bias field can be used for the development of reconfigurable microwave magnetic materials.

5. Classification of Magnetic Skyrmions

Magnetic skyrmions are topologically nontrivial inhomogeneous magnetization configurations on the nanoscale. They attracted much attention recently due to their potential applications in information recording and signal processing. Understanding the physical properties of magnetic skyrmions is important for fundamental research with the aim to develop new spintronic devices.

The arrays of chiral Bloch skyrmions in the form of 2D triangular lattices have been observed in films of cubic B20 compounds (MnSi, FeGe etc.) below the room temperature and for finite applied magnetic fields [51]. The concept of individual magnetic skyrmion stabilization in ultrathin multilayer films and dots ferromagnet/heavy metal (with a strong spin-orbit interaction) at room temperature due to interface induced DMI was suggested in Refs. [51, 52]. Such DMI favors stabilization of the chiral Neel skyrmions with a given sense of the magnetization rotation (chirality) determined by the sign of the DMI parameter D [53, 54]. If we denote the magnetization $\mathbf{m}$ components in the cylindrical coordinate system as $\mathbf{m} = (m_\rho, m_\phi, m_z)$, then the skyrmion chirality is $C = sign(m_\varphi)$ for the Bloch skyrmions and $C = sign(m_\rho)$ for the Neel skyrmions. Skyrmions with the magnetic energy depending on the sign of the product CD are called chiral skyrmions. The skyrmion chirality is determined by the phase angle Φ_0 in the expression $\Phi = q\varphi + \Phi_0$, while the parameter q stands for the skyrmion vorticity, which is always $q = 1$ for any 2D magnetic skyrmions.

The individual magnetic skyrmions in restricted geometry have attracted considerable attention of researchers assuming potential applications in spintronic devices because the skyrmion motion can be controlled by ultralow density spin-polarized current [51, 52]. These individual Neel skyrmions were recently observed at room temperature by Boulle *et al.* [55], Moreau-Luchaire *et al.* [56], and Woo *et al.* [57] in ultra-thin films and dots). The Bloch bubble-skyrmions in magnetic dots can be also stabilized without DMI and applied out-of-plane magnetic field within some range of the uniaxial magnetic anisotropy [58]. At the same time, some finite value of the DMI strength is necessary for stabilization of a single Neel skyrmion in ultrathin films and dots. The chiral skyrmions can be further stabilized by external out-of-plane magnetic field [55-57]. Temperature is usually considered to be detrimental to skyrmion stability, leading to either the transformation of the skyrmion state into a more energetically favorable state [59] or to nucleation of multiple skyrmions and labyrinth domains [55-57].

To achieve efficient manipulation of nanosized spin

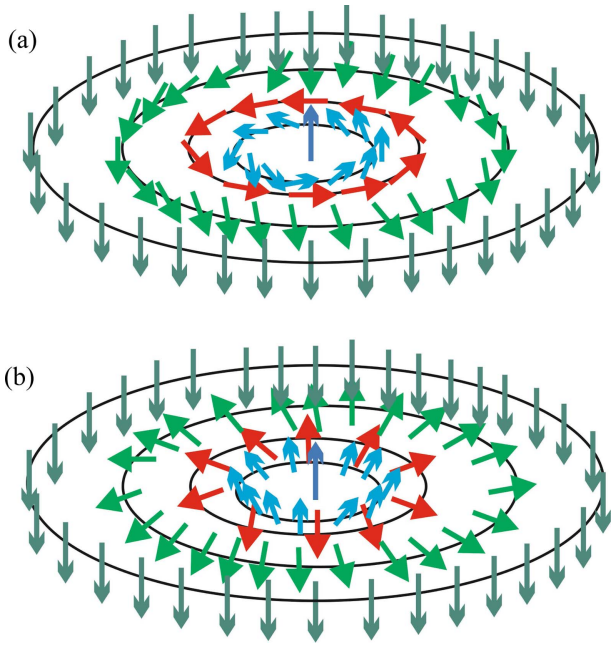

Fig. 8. (Color online) The magnetization configurations of the Bloch (a) and Neel (b) skyrmions [80].

textures and to realize skyrmion-based low energy consumption spintronic devices, it is essential to understand the magnetic skyrmion stability and dynamics in confined geometries, for instance, in ultrathin magnetic nanodots and stripes.

6. Stability of Magnetic Skyrmions

The stability and sizes of chiral skyrmions in ultrathin magnetic films were calculated accounting for the isotropic exchange, Dzyaloshinskii–Moriya exchange interaction, and out-of-plane magnetic anisotropy within micromagnetic approach. The Bloch skyrmions in magnetic films with B20 cubic crystal structure and Neel skyrmions in ultrathin films and multilayers Co/X (X = Ir, Pd, Pt) were considered. The skyrmions can be stabilized due to two different mechanisms, primary DMI or primary magnetostatic interaction, leading to small and large size skyrmions, respectively.

Conventionally, magnetic skyrmions are stabilized by chiral bulk DMI in non-centrosymmetric B20 bulk crystals/films (at low temperatures) or interfacial DMI in ultrathin magnetic films with out-of-plane magnetic anisotropy (at room temperature), respectively. The skyrmion stability in the ultrathin films relies on a delicate balance of their material parameters that are hard to control experimentally. Typically, it is more difficult to stabilize the skyrmions in comparison with magnetic vortices.

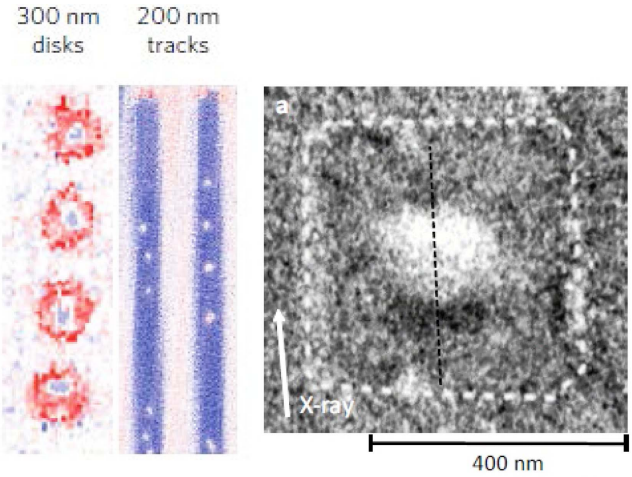

Fig. 9. (Color online) X-ray images of the Neel skyrmions in ultrathin multilayer Ir/Co(0.6 nm)/Pt [56] and Pt/Co(1 nm)/MgO [55] films and dots. The contrast corresponds to the skyrmion out-of-plane magnetization component.

6.1. Stabilization by the Dzyaloshinskii-Moriya exchange interaction

The magnetic skyrmion stability in ultrathin magnetic multilayer nanodots with interfacial DMI was simulated in Ref. [60]. It was found that two kinds of the skyrmions can be stable simultaneously in the same nanodot. In presence of the lateral confinement the magnetostatic energy significantly influences the skyrmion stability and leads to stabilization of large-radius skyrmion even at low values of the DMI strength, in addition to small-radius skyrmion stabilized by DMI. In particular, stabilization of the skyrmions with two different radii (bi-stability) is found in dipolarly-coupled $(Pt/Co/Ir)_n$ circular nanodots with the number of repeats of the unit cell n = 3 and 5. The bi-stability range is located at the DMI strength of 0.9-1.1 mJ/m^2 or at the total Co-layer thickness of 2.2-2.6 nm. The bi-stable skyrmions can be obtained in magnetic dots with realistic values of the dot sizes and DMI, exchange and anisotropy parameters. The results open a new route to developing a more efficient skyrmion memory, where information is coded as a skyrmion equilibrium size.

The stability of the Neel skyrmions in ultrathin circular magnetic nanodots was calculated analytically and simulated micromagnetically considering typical magnetic and geometrical dot parameters in Ref. [61]. The diagram of single Néel skyrmion stability/metastability, skyrmion sizes and magnetization profiles were found. Most of the skyrmions are unstable or metastable and the stability region where the Néel skyrmion is the dot ground state is small. The Dzyaloshinskii criterion for the instability of ferromagnetic state in bulk ferromagnets with respect to

the increasing DMI strength should be essentially modified to describe the stability of magnetic skyrmions in 2D systems like ultrathin ferromagnetic films and nanodots.

The quality parameter $Q = 2K/\mu_0 M_s^2$ defining the effective out-of-plane dot magnetic anisotropy is important for the skyrmion stabilization along with the DMI strength D. The cases $Q < 1$, $Q > 1$ lead to qualitatively different skyrmion magnetization profiles and conditions for the Néel skyrmion stabilization [61]. The skyrmion magnetization profiles are similar to the radial vortex profiles for $Q < 1$, Belavin-Polyakov soliton profiles at $Q \approx 1$ and bubble domain walls at $Q > 1$. The Néel skyrmion state in ultrathin circular dots can be metastable or stable even at $Q < 1$ if the DMI strength is large enough. The area of the skyrmion metastability in small radius nanodots is the largest for $Q \approx 1$. Skyrmions can be metastable if the DMI strength is $D \approx D_c$, where D_c is the modified Dzyaloshinskii critical value. This range is wide for small radius dots, $0.5 \le D/D_c \le 1.5$, and relatively narrow, $0.6 \le D/D_c \le 1$, for large radius dots. The simulated metastability/stability regions of the Néel skyrmion state essentially depend on all micromagnetic parameters, including the exchange stiffness A as well as the dot radius.

The areas of the single-Néel skyrmion stability/instability and skyrmion radius are determined as functions of the uniaxial out-of-plane magnetic anisotropy and DMI strength in Ref. [62]. It is shown that the well-known criterion of skyrmion stability in infinite film should be changed to describe the stability in nanodots. Almost all calculated Néel skyrmions in ultrathin circular nanodots are metastable. The skyrmion stability area is relatively small in terms of the dot magnetic parameters D and Q. The skyrmions are metastable if the DMI strength is $D < D_c(Q)$, where D_c is the DMI critical value, and stable (the nanodot ground state) if $D > D_c(Q)$. The function $D_c(Q)$ has a deep minimum at $Q \approx 1$ that allows optimizing the ultrathin dot magnetic parameters to stabilize the Néel skyrmions. The skyrmion stability area is extended by decreasing the out-of-plane magnetic anisotropy.

The generalized DeBonte ansatz was used to describe the inhomogeneous skyrmion magnetization in Ref. [63]. The single skyrmion metastability/instability area, skyrmion radius, and skyrmion width are found analytically as a function of reduced DMI strength, $d = Dl/A$. It is shown that the single chiral skyrmions are metastable in infinite magnetic films below a critical value of DMI d_c, and do not exist at $d > d_c$. The calculated skyrmion radius increases as d increases and diverges at $d \to d_c - 0$, whereas the skyrmion width increases monotonically as d increases up to d_c without any singularities. $d_c = 4/\pi$ or $D_c = 4A/\pi l$ in absolute units, A is the material exchange stiffness, and $l = \sqrt{A/(K_u - \mu_0 M_s^2/2)}$ is the exchange length. The calculated skyrmion width is essentially smaller than one calculated within the generalized domain wall model. The generalized DeBonte ansatz is a very good approximation to calculate the skyrmion radius, width, and energy. The Néel skyrmions can be the ground state for dots of a finite radius [62], whereas they can only be metastable in

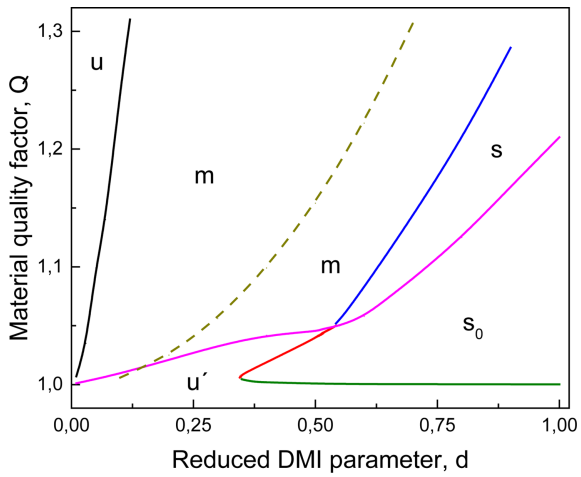

Fig. 10. (Color online) Phase diagram of the Neel skyrmion stability in ultrathin circular dot. The reduced dot radius is $R/l_{ex} = 20$. The skyrmion is the ground state in the areas s and s_0. $Q = 2K_u / \mu_0 M_s^2 \ge 1$ is the quality factor, $d = |D|l_{ex}/A$ is the reduced DMI strength. The dark yellow dashed line describes the critical line of the skyrmion metastability calculated within domain wall model in infinite film [53].

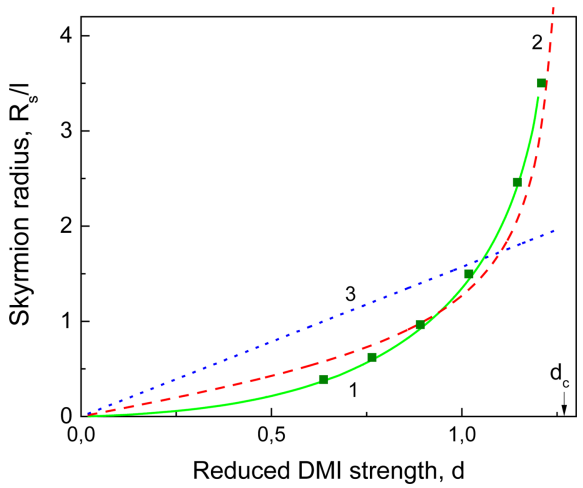

Fig. 11. (Color online) The skyrmion radius in units of $l = \sqrt{A/K}$ vs. the DMI strength, $d = |D|l/A$ in an infinite magnetic film [63]: 1 - generalized DeBonte ansatz (solid green line), 2 - generalized DW ansatz [100] (dashed red line), 3 - linear ansatz (dotted blue line). The radius obtained from numerical minimization of the skyrmion energy is shown by deep green squares.

infinite films.

6.2. Stabilization by the magnetostatic interaction

The influence of the magnetostatic interaction in circular nanodots on stability of the skyrmion magnetization configurations was considered in Ref. [59]. An uniaxial out-of-plane magnetic anisotropy was accounted. It is shown that the skyrmion state can have magnetic energy lower than the vortex and perpendicular single domain state in a finite range of magnetic anisotropy fields at room temperature even in the case of absence of the Dzyaloshinskii–Moriya exchange interaction and external magnetic field. The Bloch skyrmion is the ground state of a circular ferromagnetic nanodot without DMI and bias magnetic field for moderate out-of-plane magnetic anisotropy fields H_a ($Q < 1$) within the range $H_{c1} < H_a < H_{c2} < \mu_0 M_s$. The critical anisotropy fields of the skyrmion stability $H_{c1,2}(L, R)$ are functions of the dot thickness L and radius R.

6.3. Effects of finite temperature and magnetic field

A universal model based on the micromagnetic formalism was used to study skyrmion size and stability as a function of magnetic field and temperature in ultrathin, circular dots in Ref. [64]. The magnetic skyrmions with a small radius (compared to the dot radius) are always metastable, while large radius skyrmions form a stable ground state. The change of energy profile determines the weak (strong) size dependence of the metastable (stable) skyrmion as a function of temperature and/or field. The theoretical framework combines a proper skyrmion ansatz with thermal scaling relations of the micromagnetic parameters A, K_u, and D obtained by atomistic spin dynamics. The strong temperature dependence of the skyrmion radius occurs because the thermal evolution of an initially metastable skyrmion brings it toward the region where the skyrmion is the ground state due to increase of the DMI strength. The obtained results, corroborated by extensive simulations, provide a tool, the Q-d phase diagram, to determine the transition from the metastable to ground-state skyrmion configuration, as well as the skyrmion size in the presence of out-of-plane external field and temperature.

Micromagnetic simulations and analytical calculations were performed to study the size of the Néel skyrmion confined in a cylindrical ultrathin dot as function of out-of-plane magnetic field in Ref. [65]. There are two different types of skyrmions (large and small size) with distinct dependence of their radius on the applied out-of-plane field. The large radius skyrmions are rare, stable at zero field and possess strong and continuous dependence of their radii on the applied out-of-plane field and dot size. These skyrmions undergo a transition between stable and metastable states. In the metastable state their size dependence on the applied field becomes weak. In the other more frequent case, the skyrmions have small radius at zero field and are always metastable. They are characterized by a weak dependence of their radius on the field until a critical field is reached at which the radius increases suddenly. The skyrmion energy is bi-stable close to this critical field and there is co-existence of small and large size metastable skyrmions within some field interval. The calculated universal behavior of the Néel skyrmions in ultrathin dots with interface DMI opens a possibility to detect experimentally the skyrmion metastability/stability just looking at the skyrmion radius dependence on the applied out-of-plane magnetic field. It was found that the hysteresis is a property of metastable skyrmions only.

6.4. Artificial skyrmions in patterned nanostructures

Static magnetization configurations of thin, circular, soft magnetic nanodots, coupled to a hard antidot matrix with perpendicular magnetization, were studied by micromagnetic simulations in Ref. [66]. The dipolar coupling with the matrix can substantially enlarge the region of vortex stability in circular nanodots to the range of ultrathin thicknesses and sub-100 nm diameters. The main impact is produced by the radial component of the antidot stray field, which leads to appearance and stabilization of the magnetic vortices with unconventional textures. The vortex magnetization configuration can be tuned by a proper choice of geometrical parameters of the patterned film. Depending on the geometry and antidot-matrix material, it is possible to stabilize either a radial vortex (Neel skyrmion) or unconventional vortices with the helicity $\Phi_0 \neq 0, \pi/2, \pi$. In the case of a sufficiently thick matrix and thin dots, the radial vortices are formed, and unconventional curled vortices are stabilized otherwise.

It was demonstrated [67] that magnetic skyrmions can be stabilized in a soft ferromagnetic film, provided that it is coupled to a hard magnetic antidot matrix by exchange and dipolar interactions, without any DMI. In this nanostructure, interlayer exchange is responsible for the soft layer magnetization direction away from the antidot (out-of-plane direction). The radial component of the stray field generated by the antidot plays a crucial role in the formation of inhomogeneous magnetization configurations in the soft layer, the radial Néel skyrmions. The proposed patterned nanostructure allows for the stabilization of topologically nontrivial magnetization configurations for antidots as small as 40 nm in diameter. Depending on the material and geometric parameters, it is possible to achieve

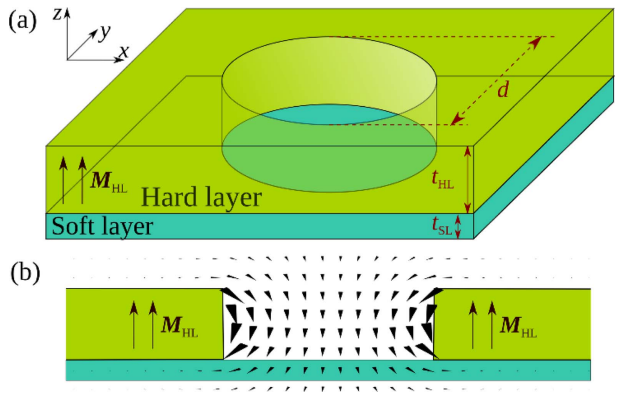

Fig. 12. (Color online) Patterned magnetic film to stabilize Neel-like skyrmions [67]. (a) The nanostructure consists of a soft magnetic layer underneath of a hard magnetic antidot matrix with perpendicular magnetization. (b) Cross-section showing the distribution of the stray magnetic field created by the hard layer.

the formation of stable Néel skyrmions at remanence, or curled solitons resembling an intermediate state between the Néel and Bloch skyrmions. The formation of the curled solitons is a result of the competing demagnetizing and Zeeman energy contributions to the stray field created by the antidot matrix. The curled skyrmions are realized in the case of relatively thin hard layers and large antidot radii, while smaller antidots and thicker hard layers support the formation of Néel skyrmions.

Magnetic skyrmions and the artificial room-temperature skyrmion crystals [68-71] can be also stabilized in patterned films without any DMI by moderate out-of-plane magnetic anisotropy [59] or dynamically [72], etc.

7. Magnetic Skyrmion Dynamics

7.1. Gauge and emergent electromagnetic fields

The concept of non-Abelian gauge fields for the description of magnetic soliton excitations was used in Ref. [73]. The component of the gauge field vector potential along the soliton local magnetization (Abelian part of the gauge potential) determines the dynamics of spin fluctuations over the soliton background in a ferromagnet. The assumption that the gauge field is a pure gauge allows calculating the gauge field components and finding simple expressions for the emergent electromagnet fields related to the soliton motion. The longitudinal component of the potential along the soliton magnetization direction (the Abelian component) enters the magnetization equations of motion of solitons and magnons determining the emergent U(1) electromagnetic field. The magnetic component of the emergent field determines the soliton topological charge (skyrmion number). The skyrmion number results in non-zero gyrovector and existence of the skyrmion gyrotropic mode and skyrmion Hall effect. The electric component of the emergent field is responsible for a spin motive force [74] and leads, in particular, to additional contribution to the magnetization damping [75]. The emergent electromagnetic field is a result of non-Abelian character of the gauge field induced by the moving magnetic soliton. The gauge field leads to an interaction of the soliton background with spin waves represented by spatial and time derivatives of the soliton magnetization.

7.2. Topological Hall effect and skyrmion Hall effect

The topological Hall effect and skyrmion Hall effect are direct consequences of the skyrmion non-zero topological charge. The current- or magnetic field driven motion of 2D topological magnetization texture experiences a transverse deflection analogous to charged particles in the classical Hall effect, or so called skyrmion Hall effect. Although the magnetic soliton (vortex, skyrmion) motion in the direction perpendicular to a driving force (velocity) is an evident consequence of the non-zero skyrmion gyrovector and existence of the gyroforce or Magnus force, the skyrmion Hall effect was experimentally observed relatively recently. It was done by Jiang *et al.* [76] and Litzius *et al.* [77] in Ta/CoFeB/TaO and Pt/CoFeB/MgO multilayers, correspondingly. To explain the skyrmion Hall effect a finite damping in the Thiele equation of motion [1] of the skyrmion center should be accounted along with the gyrovector.

In metallic ferromagnets, the emergent magnetic field of skyrmions causes a transverse deflection of itinerant electrons known as the topological Hall effect. The effect depends solely on the topology of the inhomogeneous magnetization texture and does not rely explicitly on spin-orbit coupling nor on any real magnetic flux penetrating through the sample [78]. The Hall resistivity contains contribution proportional to the skyrmion number given by Eq. (1). It was measured that the topological-Hall resistivity scales with the isolated-skyrmion density in Ir/Co/Fe/Pt multilayers over a wide range of temperature and magnetic field [79] in qualitative agreement with the theory. Nevertheless, detailed quantitative analysis showed much larger topological-Hall resistivity than the prevailing theory predicts for the observed skyrmion density [79].

7.3. Gyrotropic modes in thin and ultrathin dots and films

The main features of the dynamics of magnetic skyrmions in nanodots including the spectra of spin waves and gyrotropic modes of an isolated skyrmion were calculated by using the Landau-Lifshitz equation of the magnetization

motion [80]. The classification of the excitation modes of a skyrmion state was performed. The gyrotropic mode has the lowest frequency in the excitation spectrum and is localized in the central area of nanodot. The estimation of the gyrotropic mode frequency is important, in particular, for the processes of dynamic switching in the skyrmion polarity, which is implemented through the gyrotropic mode excitation.

The gyrotropic modes of the skyrmion ground state in ultrathin cylindrical magnetic dots were considered in Ref. [81]. The gyrotropic frequencies of the Bloch- and Neel-type magnetic skyrmions are calculated in the GHz range as a function of the skyrmion equilibrium radius, dot radius, and the dot magnetic parameters. The magnetostatic interaction is explicitly accounted via appropriate ansatz of the skyrmion magnetization. The magnetostatic interaction plays important role either in the skyrmion state stabilization or in the skyrmion low frequency gyrotropic dynamics.

Recent findings concern collective spin excitation spectra of the skyrmion lattices that demonstrate asymmetry of clockwise (CW) and counter-clockwise (CCW) skyrmion motions. Mochizuki [82] simulated one breathing mode (oscillations of the skyrmion radius) and two rotational modes (CW and CCW) in a skyrmion crystal within the GHz frequency range. The microwave measurements [83, 84] confirmed existence of only one of the skyrmion rotating modes and a breathing mode. Contrary, two rotating spin eigenmodes and one breathing skyrmion mode were detected by time-resolved magneto-optics in Cu_2OSeO_3 [85]. Recent broadband ferromagnetic resonance measurements [86] of MnSi, FeCoSi and Cu_2OSeO_3 showed existence of only two excitation modes in the spectra of these low temperature skyrmion crystals.

Single gyrotropic mode, several breathing and non-symmetric skyrmion shape modes in infinite thin films were numerically found by Lin *et al.* [87]. The skyrmion gyrotropic mode excited by the spin polarized current in a nanopillar was simulated by Zhang *et al*. [88] and Garcia-Sanchez *et al.* [89].

The skyrmion gyrotropic frequency in magnetic dots has not been clearly observed yet. An exception is the experiment by Buettner *et al.* in CoB/Pt multilayer dots [90], who found two wide resonance peaks and interpreted them as the skyrmion gyrotropic modes. The reason for that is the limited stability of skyrmions in ultrathin ferromagnetic dots. Another difficulty is a large value of the magnetization damping (the resonance linewidth) in ultrathin Co films and dots that does not allow applying a precise ferromagnetic resonance technique for the gyrotropic frequencies detection in the skyrmion state.

7.4. Collective gyrotropic modes in a dot chain

An approach that allows calculate the low frequency excitation spectrum of magnetostatically coupled skyrmions in a long dot chain was presented in Refs. [91, 92]. Skyrmion configurations in the dots (with thickness about of 1 nm and radius about of 100 nm) were stabilized by interplay of isotropic exchange and DMI, magnetic anisotropy and magnetostatic interactions, while external drives induce the skyrmion gyrations. The dipolar and quadrupolar interactions between moving skyrmions in the dots are prevailing mechanism responsible for dynamic interdot magnetostatic coupling. The approach enables to analyze collective dynamics of gyrating skyrmions for a wide range of parameters and to tune the skyrmion group velocity and frequency bandwidth. The differences in the dynamic responses of the Bloch and Neel skyrmions were demonstrated and a method allowing to recognize the type of a skyrmion (Bloch or Neel) on the base of measurements of ferromagnetic resonance frequency of such patterned film was suggested. The interdot magnetostatic coupling and frequency bandwidth are maximal for the large-radius Bloch skyrmions in the relatively thick dots.

The studies of the high-frequency excitation spectrum of skyrmions in a nanodot have shown that the azimuthal spin waves propagating on the skyrmion background are characterized by asymmetry with respect to mode rotation sense, the frequencies and profiles of azimuthal CW and CCW modes are different. A distinctive feature of the dynamics of isolated skyrmions in circular nanodots is that the excitation spectra, both low-frequency (skyrmion core gyration) and high-frequency (spin waves), are identical for the Bloch and Neel skyrmions.

Collective excitations in a linear chain of touching magnetic nanodots in a skyrmion magnetic configuration were studied in Ref. [93]. By spatial analysis of the magnetization amplitudes the excited spin modes of the chain were classified as breathing and gyrotropic skyrmion modes. These high- and low-frequency excitations are propagating with a negative and positive group velocity, respectively.

7.5. Azimuthal spin waves and breathing skyrmion excitation modes

The high-frequency spin excitations of the skyrmion state cylindrical magnetic dots were calculated in Ref. [94]. The skyrmion was represented as combination of two radially symmetric bubble domains. To consider the skyrmion dynamics an approximation of ultrathin domain wall between the circular domains was applied assuming that the magnetization does not depend on the thickness coordinate. The eigenfunctions/eigenfrequencies of spin

wave excitations over the skyrmion background were calculated as a function of the skyrmion radius. The developed approach allows estimating spin wave eigenfrequencies in the skyrmion state magnetic dots. An asymmetry between the propagating in the dot azimuthal CW and CCW spin waves arises due to the skyrmion topology.

The spin-wave excitations in a circular magnetic nanodot in different inhomogeneous, topologically non-trivial magnetization states, specifically, vortex and skyrmion states were studied in Refs. [95, 96]. Gradual change in the strength of out-of-plane magnetic anisotropy and DMI led to continuous phase transitions between different stable magnetic configurations and allowed for mapping of the spin modes in and between the vortex, Bloch-type skyrmion and Neel-type skyrmion states. The study elucidates a connection between the gyrotropic modes, azimuthal spin waves and breathing modes in these magnetization states and helps to understand the rich spin excitation spectrum.

Using spin-wave eigenmode mapping the origin of spin excitations on the skyrmion background was elucidated and a spin mode classification was proposed similar to that developed for the spin excitations in the magnetic vortex state dots (with $K_u = 0$) based on the azimuthal and radial mode indices (m, n) [95]. The excitation spectrum on the vortex background with large K_u is similar to that of the vortex state in a soft magnetic dot in that it has a low frequency gyrotropic mode, an $m = +1/-1$ azimuthal mode doublet, and a radial mode ($m = 0$, $n = 0$) with approximately the same frequencies. In the skyrmion state the radial mode frequency is essentially lower than the azimuthal SW frequencies and the frequency splitting between the azimuthal ($m = +1/-1$) spin-wave modes is essentially larger than one in a vortex state dot.

The spectra of high-order azimuthal spin waves in planar nanoelements were calculated in Ref. [96]. The nanodot edge localization found in the vortex state is also observed in small-sized skyrmions. However, the frequency degeneracy of the modes is different in the skyrmion states. The observed difference in the frequency systematics occurs for the dot edge localized spin waves in the vortex state, but not in the small skyrmion state. Large-sized skyrmions provide a possibility of spin wave channeling at the skyrmion edge. Skyrmion edge localization and DMI account for the relatively strong nonreciprocity of azimuthal spin waves. The frequency difference between the azimuthal spin waves propagating in opposite directions is substantial, and there is a significant frequency splitting between CW and CCW modes. Efficient coupling of azimuthally spin-wave modes with the index $|m| > 1$ to an external uniform microwave magnetic field was observed in dots of non-circular symmetry in the skyrmion state.

It was shown [97] that a skyrmion bubble motion in a circular dot can be described by introducing the bubble mass. The suggested approach allowed to calculate approximately other spin modes (radial and azimuthal spin waves) assuming their localization on the bubble edge. Further calculations and simulations [91, 95, 98] showed that this assumption is not justified for the modes having nodes in the radial direction with high radial index $n \geq 1$.

The dynamic properties (resonance frequencies and corresponding eigenmodes) of skyrmion states in thin FeGe circular dots were simulated in Ref. [99]. Several differences in the power spectral densities of incomplete skyrmion and isolated skyrmion states were detected. It was shown that neglecting the demagnetization energy contribution or ignoring the magnetization variation in the out-of-plane direction changes their resonance frequencies substantially. The properties of magnon modes localized on a ferromagnetic skyrmion were studied in Ref. [100]. It was found that the mode eigenfrequencies display three types of asymptotic behavior for large skyrmion radius R_s, namely, $\omega_0 \propto 1/R_s^2$ for the breathing mode and $\omega_m \propto 1/R_s$ and $\omega_m \propto 1/R_s^3$ for the modes with negative and positive azimuthal indices m, respectively. The magnon eigenfunction profiles were determined numerically.

According to the indices (m, n) classification of the spin wave excitation modes over inhomogeneous radially symmetric vortex/skyrmion background, there are some radially symmetric modes having the azimuthal index $m = 0$. These modes correspond to the skyrmion radius oscillations (skyrmion breathing) around an equilibrium value. By using micromagnetic simulations [98], it was shown that the several Neel skyrmion breathing modes can be excited by an out-of-plane magnetic field in circular dots in the wide frequency range 5-50 GHz. The oscillating skyrmion radius is conjugated with the skyrmion helicity Φ_0. Therefore, the skyrmion radius oscillations are immediately related with the skyrmion helicity oscillations. It was measured recently [101] that in Co/X multilayer films with the total thickness about of 50 nm even static helicity Φ_0 depends on the thickness coordinate z due to the magnetostatic interaction. The skyrmions are hybrid: Bloch-like in the middle plane and Neel-like at the top/bottom film surfaces.

The nonlinear dynamic behavior of a magnetic skyrmion in circular nanodots was studied numerically in Ref. [102]. The skyrmion core reversal can be achieved within nanoseconds using out-of-plane oscillating magnetic field. In contrast with VC reversal, the skyrmion reversal can

be described via the radially symmetric breathing modes.

The collective breathing modes in the linear skyrmion chains located along nanostrips were simulated in Ref. [103]. The breathing modes exhibit characteristic concave-down dispersions that represent the in-phase high-energy mode at zero wavenumber and the anti-phase low-energy mode at the first Brillouin zone boundary. The bandwidth increases with decreasing distance between nearest-neighboring skyrmions. The collective breathing modes propagate along the stripe with the high speed up to 700 m/s.

8. Summary

In this brief review, I considered recent advances in the field of magnetic vortices and skyrmions mainly focusing on skyrmions that can be stabilized in patterned multilayer films where ultrathin ferromagnetic layers are coupled to heavy metals with a large spin–orbit coupling. The skyrmion spin textures bear a topological charge and can be stabilized whether due to the chiral exchange interaction (DMI) or magnetostatic interaction. The static spin configurations, their stability, and the dynamics of the magnetic vortices and skyrmions in magnetic films and dots are also discussed.

Instead of the recent "*vortex boom*", which reached its maximum after discovery of the vortex core reversal induced by a small variable magnetic field [24, 25], a "*skyrmion boom*" started and continues nowadays. The "*skyrmion boom*" was started after the pioneering papers [51, 52] published in 2013, where the concept of individual skyrmions stabilization in ultrathin films ferromagnet/heavy metal with a strong spin-orbit interaction was introduced.

How it was underlined in Ref. [104], the magnetic skyrmions can be displaced by electrical current and/or magnetic field with high reliability and efficiency as needed for their use in different devices. Therefore, they can be exploited in magnetic memory, microwave oscillator and logic devices with a low energy consumption. Recent research efforts led to the discovery of the ultrathin multilayer films, in which the skyrmions are stable at room temperature and low bias magnetic field, and can be manipulated by relatively weak electrical currents [105]. Therefore, applications of magnetic skyrmions in the nanoscale devices are ahead.

Acknowledgements

K.G. acknowledges support by IKERBASQUE (the Basque Foundation for Science), and by the Spanish Ministerio de Ciencia, Innovacion y Universidades grant FIS2016-78591-C3-3-R.

References

[1] K. Y. Guslienko, J. Nanosci. Nanotechn. **8**, 2745 (2008).
[2] A. M. Kosevich, B. A. Ivanov, and A. A. Kovalev, Phys. Reports **194**, 117 (1990).
[3] K. L. Metlov and Y. P. Lee, Appl. Phys. Lett. **92**, 112506 (2008).
[4] K. L. Metlov, J. Appl. Phys. **113**, 223905 (2013).
[5] K. Y. Guslienko and A. Hoffmann, Phys. Rev. Lett. **97**, 107203 (2006).
[6] K. Y. Guslienko and A. Hoffmann, J. Appl. Phys. **101**, 093901 (2007).
[7] O. V. Sukhostavets, G. R. Aranda, and K. Y. Guslienko, J. Appl. Phys. **111**, 093901 (2012).
[8] G. N. Kakazei, M. Ilyn, O. Chubykalo-Fesenko, J. Gonzalez, A. Serga, A. Chumak, B. Hillebrands, and K. Y. Guslienko, Appl. Phys. Lett. **99**, 052512 (2011).
[9] G. A. Melkov, Y. Kobljanskyj, V. Novosad, A. Slavin, and K. Y. Guslienko, Phys. Rev. B **88**, 220407 (2013).
[10] J. Ding, G. N. Kakazei, X. Liu, K. Y. Guslienko, and A. O. Adeyeye, Sci. Reports **4**, 4796 (2014).
[11] J. Ding, G. N. Kakazei, X. Liu, K. Y. Guslienko, and A. O. Adeyeye, Appl. Phys. Lett. **104**, 192405 (2014).
[12] K. Y. Guslienko, G. N. Kakazei, J. Ding, X. M. Liu, and A. O. Adeyeye, Sci. Reports **5**, 13881 (2015).
[13] K. Y. Guslienko, O. V. Sukhostavets, and D. V. Berkov, Nano. Res. Letters **9**, 386 (2014).
[14] A. A. Awad, G. R. Aranda, D. Dieleman, K. Y. Guslienko, G. N. Kakazei, B. A. Ivanov, and F. G. Aliev, Appl. Phys. Lett. **97**, 132501 (2010).
[15] K. Y. Guslienko, S.-B. Choe, and S.-C. Shin, Appl. Phys. Lett. **76**, 3609 (2000).
[16] O. V. Sukhostavets, J. Gonzalez, and K. Y. Guslienko, Appl. Phys. Express **4**, 065003 (2011).
[17] O. V. Sukhostavets, J. Gonzalez, and K. Y. Guslienko, Phys. Rev. B **87**, 094402 (2013).
[18] S. Sugimoto, Y. Fukuma, S. Kasai, T. Kimura, A. Barman, and Y. Otani, Phys. Rev. Lett. **106**, 197203 (2011).
[19] H. Jung, K.-S. Lee, D.-E. Jeong, Y.-S. Choi, Y.-S. Yu, D.-S. Han, A. Vogel, L. Bocklage, G. Meier, M.-Y. Im, P. Fisher, and S.-K. Kim, Sci. Reports **1**, 59 (2011).
[20] O. V. Sukhostavets and K. Y. Guslienko, Appl. Phys. Express **8**, 023002 (2015).
[21] J.-Y. Lee, S. Choi, K.-S. Lee, K. Y. Guslienko, and S.-K. Kim, Phys. Rev. B **76**, 184408 (2007).
[22] K. Y. Guslienko, J.-Y. Lee, and S.-K. Kim, IEEE Trans. Magn. **44**, 3079 (2008).
[23] Y.-S. Choi, S.-K. Kim, J. Y. Lee, M. W. Yoo, K.-S. Lee, and K. Y. Guslienko, Phys. Rev. B **80**, 012402 (2009).
[24] B. Van Waeyenberge, A. Puzic, H. Stoll, K. W. Chou, T. Tyliszczak, R. Hertel, M. Fahnle, H. Bruckl, K. Rott, G. Reiss, I. Neudecker, D. Weiss, C. H. Back, and G. Schutz, Nature **444**, 461 (2006).

[25] S. Choi, K.-S. Lee, K. Y. Guslienko, and S.-K. Kim, Phys. Rev. Lett. **98**, 087205 (2007).
[26] S.-K. Kim, Y.-S. Choi, K.-S. Lee, K. Y. Guslienko, and D.-E. Jeong, Appl. Phys. Lett. **91**, 082506 (2007).
[27] K.-S. Lee, K. Y. Guslienko, J.-Y. Lee, and S.-K. Kim, Phys. Rev. B **76**, 174410 (2007).
[28] K. Y. Guslienko, K.-S. Lee, and S.-K. Kim, Phys. Rev. Lett. **100**, 027203 (2008).
[29] K. Y. Guslienko, A. N. Slavin, V. T. Tiberkevich, and S.-K. Kim, Phys. Rev. Lett. **101**, 247203 (2008).
[30] K.-S. Lee, S.-K. Kim, Y. S. Yu, Y. Choi, K. Y. Guslienko, H. Jung, and P. Fischer, Phys. Rev. Lett. **101**, 267206 (2008).
[31] G. de Loubens, A. Riegler, B. Pigeau, F. Lochner, F. Boust, K. Y. Guslienko, H. Hurdequint, L. W. Molenkamp, G. Schmidt, A. N. Slavin, V. Tiberkevich, N. Vukadinovic, and O. Klein, Phys. Rev. Lett. **102**, 177602 (2009).
[32] X. M. Cheng, K. Buchanan, R. Divan, K. Y. Guslienko, and D. Keavney, Phys. Rev. B **79**, 172411 (2009).
[33] A. V. Khvalkovskiy, A. N. Slavin, J. Grollier, K. A. Zvezdin, and K. Y. Guslienko, Appl. Phys. Lett. **96**, 022504 (2010).
[34] K. Y. Guslienko, R. Heredero, and O. Chubykalo-Fesenko, Phys. Rev. **B 82**, 014402 (2010).
[35] O. V. Sukhostavets, B. Pigeau, G. de Loubens, V. V. Naletov, O. Klein, K. Mitsuzuka, S. Andrieu, F. Montaigne, and K. Y. Guslienko, Phys. Rev. Lett. **111**, 247601 (2013).
[36] G. R. Aranda, J. Gonzalez, J. del Val, and K. Y. Guslienko, J. Appl. Phys. **108**, 123914 (2010).
[37] K. Y. Guslienko, G. R. Aranda, and J. Gonzalez, J. Phys.: Conf. Ser. **292**, 012006 (2011).
[38] K. Y. Guslienko, Journ. Spintronics and Magnetic Nanomaterials **1**, 70 (2012).
[39] F. Sanches, V. Tiberkevich, K. Guslienko, J. Sinha, M. Hayashi, and A. Slavin, Phys. Rev. B **89**, 140410 (2014).
[40] J. Kim and S.-B. Choe, J. Magnetics **12**, 113 (2007).
[41] A. Slavin and V. Tiberkevich, IEEE Trans. Magn. **45**, 1875 (2009).
[42] J. Kim and S.-K. Kim, J. Magnetics **22**, 29 (2017).
[43] F. G. Aliev, J. Sierra, A. Awad, G. Kakazei, D. Han, S.-K. Kim, V. Metlushko, B. Ilic, and K. Y. Guslienko, Phys. Rev. B **79**, 174433 (2009).
[44] A. A. Awad, K. Y. Guslienko, J. Sierra, G. Kakazei, V. Metlushko, and F. G. Aliev, Appl. Phys. Lett. **96**, 012503 (2010).
[45] K. Y. Guslienko, G. R. Aranda, and J. Gonzalez, Phys. Rev. B **81**, 014414 (2010).
[46] F. G. Aliev, A. Awad, D. Dielman, A. Lara, V. Metlushko, and K. Y. Guslienko, Phys. Rev. B **84**, 144406 (2011).
[47] K. Vogt, O. V. Sukhostavets, H. Schultheiss, B. Obry, P. Pirro, T. Sebastian, J. Gonzalez, K. Y. Guslienko, and B. Hillebrands, Phys. Rev. B **84**, 174401 (2011).
[48] A. A. Awad, A. Lara, V. Metlushko, K. Y. Guslienko, and F. G. Aliev, Appl. Phys. Lett. **100**, 262406 (2012).
[49] A. A. Awad, A. Lara, M. García Hernández, V. Metlushko, K. Y. Guslienko, and F. G. Aliev, J. Supercond. Nov. Magn. **26**, 2057 (2013).
[50] K. Y. Guslienko, G. N. Kakazei, Y. Kobljanskyj, G. A. Melkov, V. Novosad, and A. N. Slavin, New J. Phys. **16**, 063044 (2014).
[51] A. Fert, V. Cros, and J. Sampaio, Nature Nanotechn. **8**, 152 (2013).
[52] J. Sampaio, V. Cros, S. Rohart, A. Thiaville, and A. Fert, Nature Nanotechn. **8,** 839 (2013).
[53] S. Rohart and A. Thiaville, Phys. Rev. B **88**, 184422 (2013).
[54] G. Siracusano, R. Tomasello, A. Giordano, V. Puliafito, B. Azzerboni, O. Ozatay, M. Carpentieri, and G. Finocchio, Phys. Rev. Lett. **117**, 087204 (2016).
[55] O. Boulle, J. Vogel, H. Yang, S. Pizzini, D. Chaves, A. Locatelli, T. O. Mentes, A. Sala, L. D. Buda-Prejbeanu, O. Klein, M. Belmeguenai, Y. Roussigne, A. Stashkevich, S. M. Cherif, L. Aballe, M. Foerster, M. Chshiev, S. Auffret, I. M. Miron, and G. Gaudin Nat. Nanotechn. **11**, 449 (2016).
[56] C. Moreau-Luchaire, C. Moutafis, N. Reyren, J. Sampaio, C. A. F. Vaz, N. Van Horne, K. Bouzehouane, K. Garcia, C. Deranlot, P. Warnicke, P. Wohlhüter, J. M. George, M. Weigand, J. Raabe, V. Cros, and A. Fert, Nat. Nanotechn. **11**, 444 (2016).
[57] S. Woo, K. Litzius, B. Krueger, M. Y. Im, L. Caretta, K. Richter, M. Mann, A. Krone, R. M. Reeve, M. Weigand, P. Agrawal, I. Lemesh, M. A. Mawass, P. Fischer, M. Kläui, and G. S. D. Beach, Nat. Mat. **15**, 4593 (2016).
[58] S. Rohart, J. Miltat, and A. Thiaville, Phys. Rev. B **93**, 214412 (2016).
[59] K. Y. Guslienko, IEEE Magn. Lett. **6**, 4000104 (2015).
[60] M. Zelent, J. Tobik, M. Krawczyk, K. Y. Guslienko, and M. Mruczkiewicz, Phys. Stat Sol. - Rapid Res. Lett. **11**, 1700259 (2017).
[61] A. R. Aranda, A. Hierro-Rodriguez, G. N. Kakazei, O. Chubykalo-Fesenko, and K. Y. Guslienko, J. Magn. Magn. Mat. **465**, 471 (2018).
[62] K. Y. Guslienko, Appl. Phys. Exp. **11**, 063007 (2018).
[63] A. R. Aranda and K. Y. Guslienko, Materials **11**, 2238 (2018).
[64] R. Tomasello, K. Y. Guslienko, M. Ricci, A. Giordano, J. Barker, M. Carpentieri, O. Chubykalo-Fesenko, and G. Finocchio, Phys. Rev. B **97**, 060402 (2018).
[65] F. Tejo, A. Riveros, J. Escrig, K. Y. Guslienko, and O. Chubykalo-Fesenko, Sci. Reports **8**, 6280 (2018).
[66] R. V. Verba, D. Navas, A. Hierro-Rodriguez, S. A. Bunyaev, B. A. Ivanov, K. Y. Guslienko, and G. N. Kakazei, Phys. Rev. Applied **10**, 031002 (2018).
[67] D. Navas, R. V. Verba, A. H. Rodriguez, S. A. Bunyaev,

Xue Zhou, A. O. Adeyeye, O. V. Dobrovolskiy, B. A. Ivanov, K. Y. Guslienko, and G. N. Kakazei, APL Materials **7**, 081114 (2019).
[68] L. Sun, R. X. Cao, B. F. Miao, Z. Feng, B. You, D. Wu, W. Zhang, A. Hu, and H. F. Ding, Phys. Rev. Lett. **110** 167201 (2013).
[69] B. F. Miao, L. Sun L, Y. W. Wu, X. D. Tao, X. Xiong, Y. Wen, R. X. Cao, P. Wang, D. Wu, Q. F. Zhan, B. You, J. Du, R. W. Li, and H. F. Ding, Phys. Rev. B **90**, 174411 (2014).
[70] J. Li, A. Tan, K. W. Moon, A. Doran, M. A. Marcus, A. T. Young, E. Arenholz, S. Ma, R. F. Yang, C. Hwang, and Z. Q. Qiu, Nat. Commun. **5**, 4704 (2014).
[71] D. A. Gilbert, B. B. Maranville, A. L. Balk, B. J. Kirby, P. Fischer, D. T. Pierce, J. Unguris, J. A. Borchers, and K. Liu, Nat. Commun. **6**, 8462 (2015).
[72] Y. Zhou, E. Iacocca, A. Awad, R. Dumas, F. Zhan, H.-B. Braun, and J. Akerman, Nat. Commun. **6**, 8193 (2015).
[73] K. Y. Guslienko, Europhys. Lett. **113**, 67002 (2016).
[74] J.-H. Moon and K.-J. Lee, J. Magnetics **16**, 6 (2011).
[75] O. V. Sukhostavets and K. Y. Guslienko, Low Temp. Phys. **41**, 772 (2015).
[76] W. Jiang, X. Zhang, G. Yu, W. Zhang, X. Wang, M. B. Jungfleisch, J. E. Pearson, X. Cheng, O. Heinonen, K. L. Wang, Y. Zhou, A. Hoffmann, and S. G. E. te Velthuis, Nat. Phys. **13**, 162 (2017).
[77] K. Litzius, I. Lemesh, B. Krüger, P. Bassirian, L. Caretta, K. Richter, F. Büttner, K. Sato, O. A. Tretiakov, J. Förster, R. Reeve1, M. Weigand, I. Bykova, H. Stoll, G. Schütz, G. Beach, and M. Kläui, Nat. Phys. **13**, 170 (2017).
[78] P. Bruno, V. K. Dugaev, and M. Taillefumier, Phys. Rev. Lett. **93**, 096806 (2004).
[79] M. Raju, A. Yagil, A. Soumyanarayanan, A. K. C. Tan, A. Almoalem, F. Ma, O. M. Auslaender, and C. Panagopoulos. Nat. Commun. **10**, 696 (2019).
[80] K. Y. Guslienko and Z. V. Gareeva, IEEE Magn. Lett. **8**, 4100305 (2017).
[81] K. Y. Guslienko and Z. V. Gareeva, J. Magn. Magn. Mat. **442**, 176 (2017).
[82] M. Mochizuki, Phys. Rev. Lett. **108**, 017601 (2012).
[83] Y. Onose, Y. Okamura, S. Seki, S. Ishiwata, and Y. Tokura, Phys. Rev. Lett. **109**, 037603 (2012).
[84] Y. Okamura, F. Kagawa, M. Mochizuki, M. Kubota, S. Seki, S. Ishiwata, M. Kawasaki, Y. Onose, and Y. Tokura, Nat. Commun. **4**, 2391 (2013).
[85] N. Ogawa, S. Seki, and Y. Tokura, Sci. Reports **5**, 9552 (2015).
[86] T. Schwarze, J. Waizner, M. Garst, A. Bauer, I. Stasinopoulos, H. Berger, C. Pfleiderer, and D. Grundler, Nat. Mat. **14**, 478 (2015).
[87] S. Z. Lin, C. D. Batista, and A. Saxena, Phys. Rev. B **89**, 024415 (2014).
[88] S. Zhang, J. Wang, Q. Zheng, Q. Zhu, X. Liu, S. Chen, C. Jin, Q. Liu, C. Jia, and D. Xue, New J. Phys. **17**, 023061 (2015).
[89] F. Garcia-Sanchez, J. Sampaio, N. Reyren, V. Cros, and J.-V. Kim, New J. Phys. **18**, 075011 (2016).
[90] F. Buettner, C. Moutafis, M. Schneider, B. Krueger, C. M. Guenther, J. Geilhufe, C. K. Schmising, J. Mohanty, B. Pfau, S. Schaffert, A. Bisig, M. Foerster, T. Schulz, C. A. F. Vaz, J. H. Franken, H. J. M. Swagten, M. Kläui, and S. Eisebitt, Nat. Phys. **11**, 225 (2015).
[91] Z. V. Gareeva and K. Y. Guslienko, J. Phys. Commun. **2**, 035009 (2018).
[92] Z. V. Gareeva and K. Y. Guslienko, Phys. Sol. State **60**, 1146 (2018).
[93] M. Mruczkiewicz, P. Gruszecki, M. Zelent, and M. Krawczyk, Phys. Rev. B **93**, 174429 (2016).
[94] Z. V. Gareeva and K. Y. Guslienko, Phys. Stat. Sol. - Rapid Res. Lett. **10**, 227 (2016).
[95] M. Mruczkiewicz, M. Krawczyk, and K. Y. Guslienko, Phys. Rev. B **95**, 094414 (2017).
[96] M. Mruczkiewicz, P. Gruszecki, M. Krawczyk, and K. Y. Guslienko, Phys. Rev. B **97**, 064418 (2018).
[97] I. Makhfudz, B. Krueger, and O. Tchernyshyov, Phys. Rev. Lett. **109**, 217201 (2012).
[98] J.-V. Kim, F. Garcia-Sanchez, J. Sampaio, C. Moreau-Luchaire, V. Cros, and A. Fert, Phys. Rev. B **90**, 064410 (2014).
[98] M. Beg, M. Albert, M.-A. Bisotti, D. Cortes-Ortuño, W. Wang, R. Carey, M. Vousden, O. Hovorka, C. Ciccarelli, C. S. Spencer, C. H. Marrows, and H. Fangohr, Phys. Rev. B **95**, 014433 (2017).
[100] V. P. Kravchuk, D. D. Sheka, U. K. Rößler, J. van den Brink, and Y. Gaididei, Phys. Rev. B **97**, 064403 (2018).
[101] W. Legrand, J.-Y. Chauleau, D. Maccariello, N. Reyren, S. Collin, K. Bouzehouane, N. Jaouen, V. Cros, and A. Fert, Sci. Adv. **4**, eaat0415 (2018).
[102] B. Zhang, W. Wang, M. Beg, H. Fangohr, and W. Kuch, Appl. Phys. Lett. **106**, 102401 (2015).
[103] J. Kim, J. Yang, Y.-J. Cho, B. Kim, and S.-K. Kim, J. Appl. Phys. **123**, 053903 (2018).
[104] G. Finocchio, F. Büttner, R. Tomasello, M. Carpentieri, and M. Kläui, J. Phys. D: Appl. Phys. **49**, 423001 (2016).
[105] A. Fert, N. Reyren, and V. Cros, Nat. Rev. Mat. **2**, 17031 (2017).